PERGAMON

International Journal of Solids and Structures 38 (2001) 7121–7137

INTERNATIONAL JOURNAL OF SOLIDS and STRUCTURES

www.elsevier.com/locate/ijsolstr

Attenuation and speed of antiplane shear wave in fiber-reinforced composites with random interfacial cracks

Jin-Yeon Kim *

Department of Industrial, Welding and Systems Engineering, Edison Joining Technology Center, The Ohio State University, 1248 Arthur E. Adams Drive, Columbus, OH 43221, USA

Received 25 April 2000; in revised form 28 November 2000

Abstract

Effects of fiber–matrix interfacial debonding on the attenuation and speed of antiplane shear wave propagating in fiber-reinforced composites are investigated. A probabilistic approach is proposed based on the scattering analysis of a single representative fiber from randomly distributed fibers with random interfacial cracks. The average total cross-section of the representative fiber is obtained using assumed probability distributions, and then the causal differential method is applied to calculate the effective wave speed and coherent attenuation. For a composite with low fiber volume fraction, the results are compared with those from other theories. When the mean crack size exceeds a certain subtending angle, the interfacial debonding affects significantly dynamic behaviors of the composite. The attenuation changes mainly in low frequency region quite sensitively to the variance of the crack length, whereas the variation of wave speed takes place in the whole frequency range considered.

Keywords: Effective wave speed; Attenuation; Interfacial crack; Fiber debonding; Fiber-reinforced composites; Multiple scattering

1. Introduction

It is well known that the mechanical behavior of fiber-reinforced composites is influenced significantly by the fiber–matrix interfacial bonding quality. The partial debonding due to insufficient fiber–matrix adhesive force can cause interfacial arc-shaped cracks whose orientation and size distributions are random. The interfacial debonding is inevitable in the ceramic fiber–metal matrix composites because of the inherently poor adhesion between the metal and the ceramic. It has been reported that the interfacial debonding is the dominant failure mechanism of the metal matrix composite in the initial stage of fatigue life (Johnson, 1989) before other failure mechanisms, e.g. matrix cracking, prevail. Reduction of the static effective stiffness due to imperfect interfaces has been studied extensively based on the models employing the interfacial crack or thin interphasal layers. The results of these studies show that the overall stiffness of the composite decreases gradually with the increase of interfacial imperfectness (Teng, 1992; Kim et al., 1995;

* Fax: +1-614-292-6842.
E-mail address: kim.896@osu.edu (J.-Y. Kim).

0020-7683/01/$ - see front matter
PII: S0020-7683(00)00424-8

Yuan et al., 1997). It is expected that the dynamic behavior would be more complicated than the static case because of the frequency dependent interaction of elastic wave with the interfacial cracks.

In the nondestructive evaluation of composite materials, the ultrasonic wave introduced into the composite is modified by the internal microstructure such as fiber shape, fiber arrangement and fiber–matrix interface condition. However, most of the previous theoretical studies to evaluate the effective composite properties assume the perfectly bonded interface. To better understand dynamic behaviors of the actual composite, one needs to implement a theoretical model in which the realistic microstructures affecting the wave propagation are taken into account. In this point of view, the interfacial debonding may be the first important parameter to be included. Yang and Norris (1991) have analyzed the scattering of elastic waves from the partially debonded elastic cylinder. They studied the change of scattering cross-section with respect to the debonding angle as well as the low frequency Helmholtz resonance that can be excited when the neck joining the matrix and the fiber is very small. Benveniste and Aboudi (1984) used the semi-analytical cell method to predict the decrease of wave speed in a composite with fiber–matrix debonding. Most recently Liu and Kriz (1997) studied multiple scattering of shear wave and effective properties of a composite with aligned interfacial cracks. They reported anomalous jumps in shear modulus and corresponding sharp peaks in attenuation.

In this paper, the effects of interfacial debonding on the propagation of antiplane shear wave in fiber-reinforced composites are studied. A probabilistic approach based on the single scattering solution is proposed to evaluate the dispersion and attenuation of the composite with randomly debonded fibers. The analysis is performed for a representative fiber that describes probabilistically the randomness of the interfacial crack. The average total cross-section of the representative fiber is obtained. The causal differential method of Beltzer and Brauner (1985, 1986 and 1987) is then applied to calculate of the wave speed and attenuation using the average total cross-section. The results are compared with those from the Waterman and Truell (1961) and independent scatterer theory. The effects of crack size and distribution are illustrated in numerical results for varying mean value and variance of the crack size.

2. Theory

2.1. Scattering analysis for a fiber with random interfacial crack

In order to predict the dynamic properties of a composite with debonded fibers it is required to analyze the wave scattering by the multiple fibers with random interfacial cracks. The probabilistic multiple scattering theory, for example, Bose and Mal (1973), can be applied for this purpose. As an alternative approach, the model based on the single scattering analysis can be used. In this approach a representative scattering object is considered that reflects all characteristics of scatterer in probabilistic or deterministic manners. For example, when the length and orientation of the crack are different from a fiber to the other, these parameters in the representative scatterer are treated as random variables. As shown in Fig. 1, a fiber with interfacial debonding is taken as a representative scattering object. The physical quantities associated with the scattering are evaluated probabilistically by averaging them over the ranges of distributions.

Now consider a two-phase composite containing an elastic cylindrical fiber embedded in an infinite medium. The shear modulus and mass density of the matrix are denoted by μ_1 and ρ_1 and those of the fiber by μ_2 and ρ_2. Both fiber and matrix are assumed to be isotropic and homogeneous. From now on, subscripts 1 and 2 denote exterior and interior of the fiber, respectively. When the attenuation due to either viscosity or incoherent scattering is present, the energy absorption can be accounted for using complex shear modulus whose imaginary part becomes the loss modulus. It is assumed that each inclusion has a crack at its interface with the host medium, and the crack size δ in subtending half angle and the crack orientation angle θ_o are different at each fiber as illustrated in Fig. 1. The orientation of the crack is

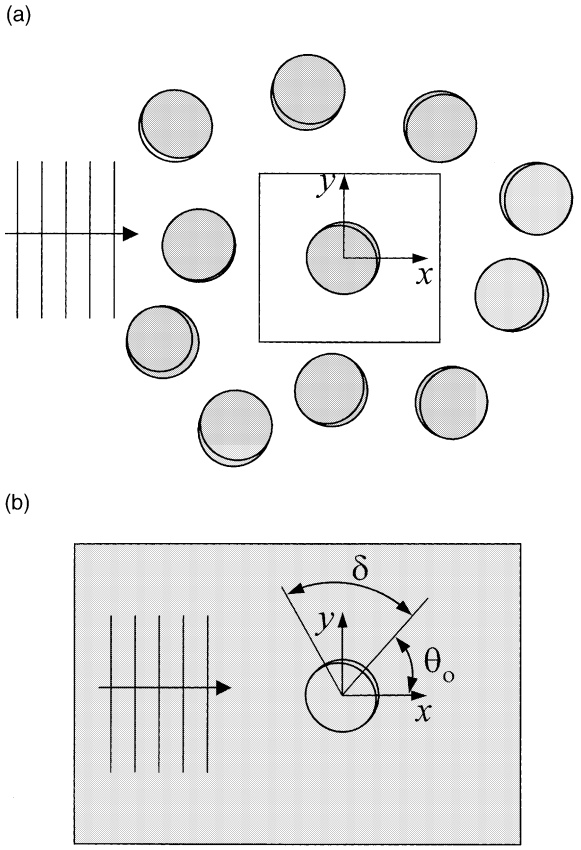

Fig. 1. Antiplane shear wave propagation in fiber-reinforced composite with debonded interfaces: (a) wave propagation in a composite with randomly debonded interface, (b) single representative fiber.

assumed to be equally probable in $(-\pi, \pi)$. It is noted that under this assumption the effective medium remains transversely isotropic.

Suppose a plane time-harmonic antiplane shear wave displacement normally incident to the fiber,

$$u^{\text{inc}} = A\exp(\mathrm{i}k_1 r\cos\theta), \tag{1}$$

where $k_1(=\omega/c_1)$ denotes the wave number and $c_1(=(\mu_1/\rho_1)^{1/2})$ the shear wave speed in the matrix. The time dependence, $\exp(-\mathrm{i}\omega t)$ is suppressed for brevity. An equivalent scattering problem is considered, which is obtained by rotating the coordinate system to have the crack orientation aligned with the rotated x-axis as shown in Fig. 2. When the incident angle changes to $-\theta_o$, the incident wave in the rotated coordinate system is written as

$$u^{\text{inc}} = A\exp[\mathrm{i}k_1 r\cos(\theta+\theta_o)]. \tag{2}$$

The scattered field can be represented as a sum of the scattered fields in the absence and in the presence of the interfacial crack. The interior field can also be represented in the same way:

$$u_1 = u^{\text{inc}} + u_1^{(0)} + u_1^{(1)}, \tag{3}$$

$$u_2 = u_2^{(0)} + u_2^{(1)}. \tag{4}$$

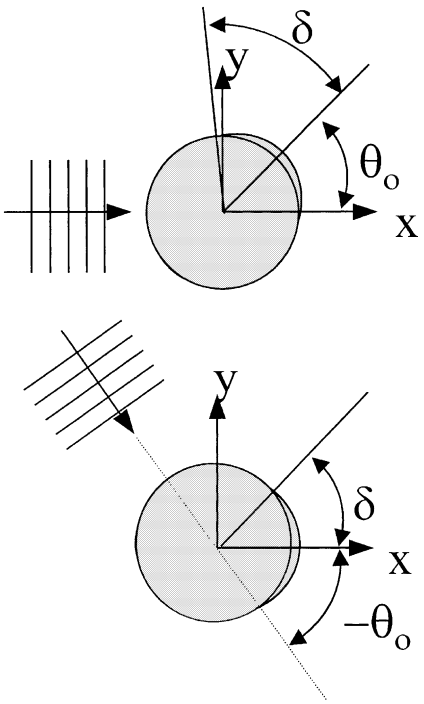

Fig. 2. Equivalent scattering problems.

The additional fields due to the presence of the interfacial crack can be split further into the symmetric and antisymmetric fields (Yang and Norris, 1991),

$$u_{1,2}^{(1)} = u_{1,2S}^{(1)} + u_{1,2A}^{(1)}, \tag{5}$$

These fields are expanded in terms of eigenfunctions in cylindrical coordinate system, and then the symmetric and antisymmetric parts of the scattered field are

$$u_{1S}^{(1)} = \sum_{n=0}^{\infty} E_n^{(S)} H_n^{(1)}(k_1 r)\cos n\theta, \tag{6}$$

$$u_{1A}^{(1)} = \sum_{n=1}^{\infty} E_n^{(A)} H_n^{(1)}(k_1 r)\sin n\theta, \tag{7}$$

where $E_n^{(S),(A)}$ means coefficients for the additional scattered field, thus are functions of θ_o and δ, and $H_n^{(1)}(x)$ denotes the first kind Hankel function of order n. The solution procedure is summarized in Appendix A.

In order to calculate the wave speed and attenuation of the effective medium using the causal differential method, the total cross-section (scattering plus absorption cross-sections) of the representative fiber is needed. The ordinary total cross-section of a scattering object in the lossless elastic medium can be described in terms of the scattering coefficients according to the forward scattering (or optical theorem) (Morse and Feshbach, 1953). When the scattering happens in the lossy medium, the total scattering is defined as a quantity proportional to the total power abstracted due to the scattering as well as the absorption of the lossy host medium. It is noted that the ordinary forward scattering theorem for the lossless medium is still valid for the scattering in the lossy medium (Bohren and Gilra, 1979) if the absorption of the

medium is taken into account with complex wave number. Therefore, the total cross-section (γ^{tot}) is given by

$$\gamma^{\mathrm{tot}}(\omega) = -\mathrm{Re}\left[\frac{4}{k_1}F(\theta)\right], \tag{8}$$

where $F(\theta)$ denotes the directional scattering amplitude. In this work, the total cross-section is represented by the scattering coefficients as:

$$\gamma^{\mathrm{tot}}(\omega) = -\frac{4}{|A|^2}\mathrm{Re}\left\{k_1^{-1}\left(\sum_{n=0}^{\infty}A_n(-\mathrm{i})^n + E_0^{(\mathrm{S})} + \sum_{n=1}^{\infty}(E_n^{(\mathrm{S})} + E_n^{(\mathrm{A})})(-\mathrm{i})^n\right)\right\}. \tag{9}$$

If the orientation angle and the size of the individual crack are statistically independent, the joint probability density function becomes,

$$p(\theta_{\mathrm{o}}, \delta) = p(\theta_{\mathrm{o}})p(\delta). \tag{10}$$

Moreover, if the crack orientation angle is equally probable in $(-\pi, \pi)$, the mean value of a random function (f) is calculated with probability density functions of random variables as:

$$\bar{f}(\delta) = \frac{1}{2\pi}\int_{-\pi}^{\pi} f(\theta_{\mathrm{o}}, \delta)\,\mathrm{d}\theta, \tag{11}$$

$$\langle f\rangle = \int_0^{\pi}\bar{f}(\delta)p(\delta)\,\mathrm{d}\delta. \tag{12}$$

Therefore, the average total cross-section is derived as:

$$\langle\gamma^{\mathrm{tot}}(\omega)\rangle = -\frac{4}{|A|^2}\mathrm{Re}\left\{k_1^{-1}\left(\sum_{n=0}^{\infty}A_n(-\mathrm{i})^n + \langle E_0^{(\mathrm{S})}\rangle + \sum_{n=1}^{\infty}\left(\langle E_n^{(\mathrm{S})}\rangle + \langle E_n^{(\mathrm{A})}\rangle\right)(-\mathrm{i})^n\right)\right\}, \tag{13}$$

where the average scattering coefficients $\langle E_n^{(\mathrm{S}),(\mathrm{A})}\rangle$ can be obtained from the average expansion coefficients ($\beta_m^{(\mathrm{S}),(\mathrm{A})}$) of crack opening displacement (COD) using Eq. (12),

$$\langle E_0^{\mathrm{S}}\rangle = -\frac{Z}{4}\frac{J_0'(k_2a)}{D_0}\int_0^{\pi}p(\delta)\delta\bar{\beta}_1^{(\mathrm{S})}(\delta)\,\mathrm{d}\delta, \tag{14}$$

$$\langle E_n^{\mathrm{S}}\rangle = -\frac{Z}{n}\frac{J_n'(k_2a)}{D_n}\sum_{m=1}^{\infty}\int_0^{\pi}p(\delta)J_{2m-1}(m\delta)\bar{\beta}_m^{(\mathrm{S})}(\delta)\,\mathrm{d}\delta, \tag{15}$$

$$\langle E_n^{\mathrm{A}}\rangle = -\frac{Z}{n}\frac{J_n'(k_2a)}{D_n}\sum_{m=1}^{\infty}\int_0^{\pi}p(\delta)J_{2m}(m\delta)\bar{\beta}_m^{(\mathrm{A})}(\delta)\,\mathrm{d}\delta. \tag{16}$$

To find the orientation average of COD expansion coefficients, the systems of the linear equations in Eqs. (A.14) and (A.19) are averaged over the crack orientation. Then, one has

$$\bar{N}_0^{(\mathrm{S})} = \frac{\delta}{2}\delta_{n1}J_0'(k_2a)B_0 + \sum_{p=1}^{\infty}\frac{B_p}{p}J_{2n-1}(p\delta)J_p'(k_2a), \tag{17}$$

$$\bar{N}_m^{(\mathrm{S}),(\mathrm{A})} = 0, \quad m \neq 0. \tag{18}$$

The mean antisymmetric COD expansion coefficients vanish ($\bar{\beta}_m^{(\mathrm{A})} = 0$) and thus only the symmetric part remains. Moreover, it is interesting to note that only monopole term remains as the excitation field on the

average, which holds the effective medium to be transversely isotropic. Consequently, the average total cross-section is reduced as:

$$\langle \gamma^{\mathrm{tot}}(\omega)\rangle = -\frac{4}{|A|^2}\,\mathrm{Re}\left\{ k_1^{-1}\sum_{n=0}^{\infty}\left(A_n + \langle E_n^{\mathrm{S}}\rangle\right)(-\mathrm{i})^n \right\}. \tag{19}$$

2.2. Determination of wave speed and attenuation

Among the theoretical methods to predict the wave propagation in inhomogeneous media, the causal differential method has been known to provide reasonable results up to the high frequency region regardless of comprising constituents of a composite (Kim, 1999). This method is similar to the differential effective medium approximation used widely for the estimation of static effective moduli (Norris, 1985). In the dynamic problem, the attenuation is obtained using the differential scheme and then the wave speed is calculated using the Kramers–Kronig relationship between wave speed and attenuation (Beltzer and Brauner, 1985, 1986, 1987). For the low concentration of cracks in a homogeneous isotropic solid, the attenuation and the wave speed have been analyzed by using the Kramers–Kronig relation without considering the multiple scattering effects (Angel and Achenbach, 1991; Zhang and Gross, 1993).

In the causal differential method, the multiple scattering effects are considered approximately by accumulating the sufficiently small differential increment of single scattering effect. The attenuation is calculated from the scattering by a newly added differential increment of the inclusion phase into the medium homogenized one step before. A self-consistent type homogenization is carried out assuming the attenuation of this new medium as the sum of those in matrix and newly generated by the scattering as:

$$\alpha(v_2 + \Delta v_2) = \alpha(v_2) + \frac{\Delta v_2}{2V}\langle \gamma^{\mathrm{tot}}\rangle. \tag{20}$$

where Δv_2 represents the increment in volume fraction, V the volume of inclusion, and $\langle \gamma^{\mathrm{tot}}\rangle$ the total cross-section of the associated scattering process. Once the attenuation of this new medium is determined, the wave speed is predicted resorting to the following form of the Kramers–Kronig relation among others (Weaver and Pao, 1981)

$$\frac{1}{c(\omega)} - \frac{1}{c(0)} = \frac{2\omega^2}{\pi} P\int_0^{\infty} \frac{\alpha(\Omega)\,\mathrm{d}\Omega}{\Omega^2(\Omega^2-\omega^2)}, \tag{21}$$

where $c(0)$ is the wave speed in static limit.

The procedure for numerical calculation of the above integral is summarized. When the wave speed in the geometric limit is known, the method of Angel and Achenbach (1991) can be employed. If it is not the case just like the present problem it is necessary to start from the wave speed in static limit. The principal value integral in Eq. (21) will be split into three parts,

$$P\int_0^{\infty} \frac{\alpha(\Omega)\,\mathrm{d}\Omega}{\Omega^2(\Omega^2-\omega^2)} = \left\{ \int_{\varepsilon}^{\omega-\varpi} + \int_{\omega-\varpi}^{\omega+\varpi} + \int_{\omega+\varpi}^{\infty} \right\} \frac{\alpha(\Omega)\,\mathrm{d}\Omega}{\Omega^2(\Omega^2-\omega^2)}, \quad \varepsilon, \varpi \to 0. \tag{22}$$

The singularity in the first integral can be removed by assuming the attenuation and its first derivative vanishes at $\omega = 0$. The second integral is transformed into the integrable form by the above assumption and the change of variable, that is,

$$\int_{\omega-\varpi}^{\omega+\varpi} \frac{\alpha(\Omega)\,\mathrm{d}\Omega}{\Omega^2(\Omega^2-\omega^2)} = \int_0^{\varpi} \frac{\mathrm{d}z}{z}\left(\frac{\alpha(\omega+z)}{(\omega+z)^2(2\omega+z)} - \frac{\alpha(\omega-z)}{(\omega-z)^2(2\omega-z)} \right). \tag{23}$$

In the last integral, it is assumed that there exists a large number K such that $\alpha(\omega)$ is nearly constant for all values of ω greater than K. Then the integration is approximated as (Angel and Achenbach, 1991)

$$\int_{\omega+\varpi}^{\infty} \frac{\alpha(\Omega)\,\mathrm{d}\Omega}{\Omega^2(\Omega^2-\omega^2)} \approx \int_{\omega+\varpi}^{K} \frac{\alpha(\Omega)\,\mathrm{d}\Omega}{\Omega^2(\Omega^2-\omega^2)} - \frac{\alpha(K)}{\omega^2}\left(\frac{1}{K}+\frac{1}{2\omega}\log\frac{K-\omega}{K+\omega}\right). \tag{24}$$

3. Results and discussion

The material considered in numerical calculation is SiC/Al composite. The shear modulus and mass density of the matrix are $\mu_1 = 38.0$ GPa, $\rho_1 = 2720$ kg/m^3 and those of the fiber are $\mu_2 = 188.7$ GPa, $\rho_2 = 3200$ kg/m^3. The fiber volume fraction is 40% otherwise specified. Numerical results are presented by the effective wave speed normalized by the wave speed of the matrix and the attenuation in α/k_1. The probability density functions for the crack size used in the numerical calculations are uniform and truncated Gaussian distributions that are defined in a finite range of random variable (crack size). The definition and mathematical expression of the truncated Gaussian distribution are given in Appendix B.

In Fig. 3, the wave speed and attenuation calculated with different volume increments are shown for mean debonding angle $4\pi/3$ and variance 1. Excellent convergences for both wave speed and attenuation are observed. No pronounced difference is found when the volume increment is smaller than $\Delta v_2 = 0.05$. Therefore, the volume increments are set as values under 0.05 in the following calculations. It is noted from the figures that the multiple scattering process smoothes out the undulation of wave speed and attenuation at higher frequencies and diminishes the attenuation at around the resonance frequency (Beltzer and Brauner, 1987).

In Fig. 4, the wave speed and attenuation predicted by the present method are compared with those predicted using the Waterman–Truell (WT) theory (1963) and the theory for independent scatterer. The fiber volume fraction is 15%. The probabilistic total cross-section for the single representative fiber is utilized in the WT formula. The independent scatterer theory is implemented by taking just single step of volume increment ($\Delta v_2 = 0.15$). Due to the low volume fraction, the theory of independent scatterer predicts results that are quite close to those of the present differential theory with multiple steps. On the contrary, it is noted that the wave speed from the application of WT theory deviates from others. Attenuations from different theories fall in qualitatively similar range except that WT theory predicts higher attenuation when the debonding angle is large. Similar comparisons have been reported by Beltzer and Brauner (1987).

The changes of wave speed and attenuation spectra for different debonding angles are shown in Fig. 5. Here, the variance of the debonding angle is assumed to be zero to observe the effect of solely the debonding angle on the wave speed and attenuation. The dynamic nature of the SiC/Al composite with the perfect fiber–matrix interface appears weakly dispersive. However, the presence of the interfacial debonding alters significantly the dynamic properties of the material. In contrast to the gradual degradation of static stiffness, the dispersion spectra for the different debonding angles are very complicated. When the fibers are much disengaged ($2\bar{\delta} \geqslant 3\pi/2$), the Helmholtz resonance is strongly excited and influences both dispersion and attenuation in narrow frequency band around $k_1 a = 0.4$. It can be observed that the interfacial debonding influences mainly the attenuation in the low frequency region as shown in Fig. 5(b).

In Fig. 6, the variations of the normalized wave speed and attenuation are depicted as functions of the debonding angle ($2\bar{\delta}$) for the different frequencies. The quasi-static ($k_1 a = 0.05$) wave speed decreases monotonically as the debonding angle increases. However, in the dynamic region, when the crack size exceeds a certain degree of angle depending on the frequency, the wave speed does not simply decrease. It is observed in Figs. 5 and 6, that the wave speeds at higher frequencies have their maxima around $2\bar{\delta} = \pi$. On the other hand, the attenuations in this regime have their first maxima at around $2a\bar{\delta}/\lambda = 0.4$. This implies that the wave can detect best the effect of debonding when the crack length is approximately half of the wavelength. As the crack length becomes larger than the wavelength the wave can only see the part of the

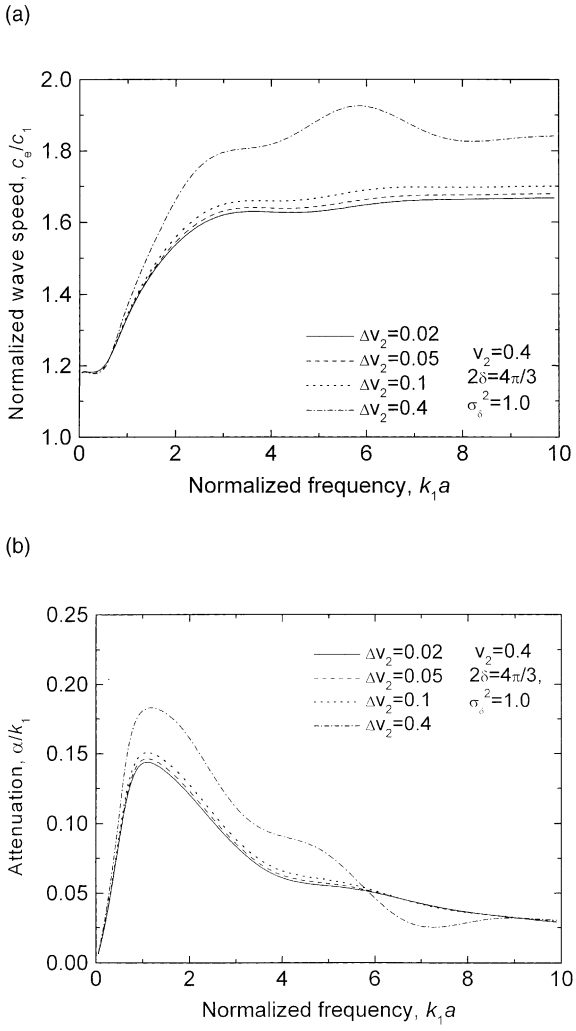

Fig. 3. Convergence of numerical integration examined with different increments of inclusion volume ($2\bar{\delta} = 120°$ and $\sigma_\delta^2 = 1$): (a) wave speed, and (b) attenuation.

fiber so that it can sense only perfect bonding or complete debonding rather than the partial debonding. It explains the reason that the attenuation in the high frequency limit is bounded by the attenuations of perfectly bonded and completely debonded fiber.

The normalized wave speed and attenuation are shown in Fig. 7 for the mean debonding angle $2\bar{\delta} = \pi$ with different variances. The crack size is distributed in the truncated Gaussian with variances $\sigma_\delta^2 = 0$, 0.05, 0.5, 1.04 and 2.09, and uniform over $0 \leqslant 2\delta \leqslant 2\pi$ and $\sigma_\delta^2 = 3.1$. The size distribution causes changes of the wave speed in the whole range of the frequency whereas its effects on the attenuation are confined in the low frequency range centered around $k_1a \approx 1$. It shifts the Helmholtz resonance frequency. The normalized wave speed and attenuation for the mean debonding angle $2\bar{\delta} = \pi/3$ for varying variance $\sigma_\delta^2 = 2$, 1, 0.2 are shown in Fig. 8. The higher variances gives rise to higher attenuation in low frequency region, while the lower variance causes slightly higher attenuation in high frequency region. In Fig. 9, those for the mean debonding angle $2\bar{\delta} = 5\pi/3$ are shown. The variance of crack size mainly controls the sharpness of the

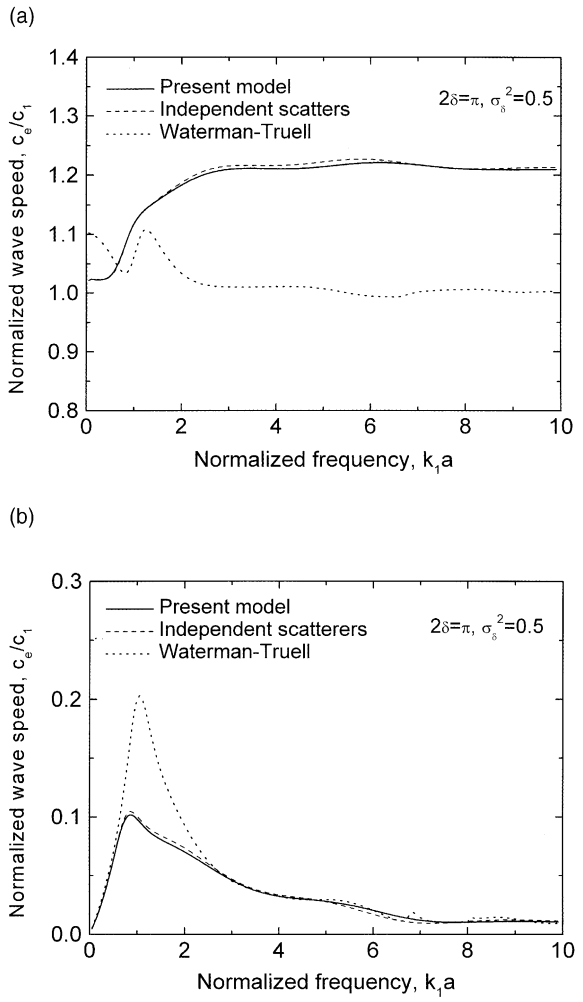

Fig. 4. Comparison of wave speeds with those from other theories for $2\bar{\delta} = 90°$ and $\sigma_\delta^2 = 0.5$: (a) wave speed, and (b) attenuation.

resonance. Two wave speeds for $\sigma_\delta^2 = 0$ and 0.2 are hardly distinguished. It is noted that the low frequency resonance still affects very much the average response of the statistical medium via the variance of the crack size. It is found from these results that the attenuation is quite sensitive to the variance of the crack size.

4. Summary

A simple analytic model is presented to calculate the shear wave propagation in the unidirectional fiber-reinforced composite containing random interfacial cracks. The randomness of crack size and orientation angle is modeled with different probability density functions. The coherent attenuation and effective wave speed are predicted using the causal differential method with the average total cross-section of the representative fiber for the random interfacial crack. Numerical results exhibit that the existence of the interfacial cracks modify significantly the wave speed in the whole range of frequency and the attenuation in the

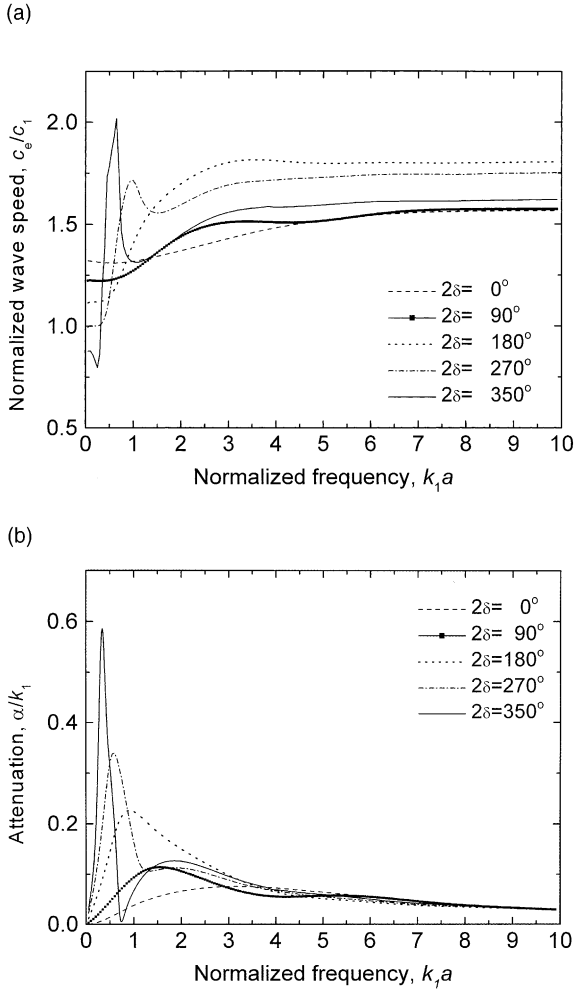

Fig. 5. Variations of wave speed and attenuation versus debonding angle: (a) normalized wave speed, (b) normalized attenuation.

frequency range of $k_1a < 3$. The variance of crack size affects in different way the wave speed and attenuation depending on the size of the crack. The attenuation is found to be very sensitive to the variance of the crack size.

Acknowledgements

The author wishes to thank Prof. Yoo, Choong-Don from KAIST, Korea for his comments and encouragement during the preparation of this paper.

Appendix A. Scattering from a single debonded fiber

For the normally incident shear wave of Eq. (2), the scattered and interior displacement fields in the absence of the interfacial crack can be written in terms of eigenfunctions in cylindrical coordinate system

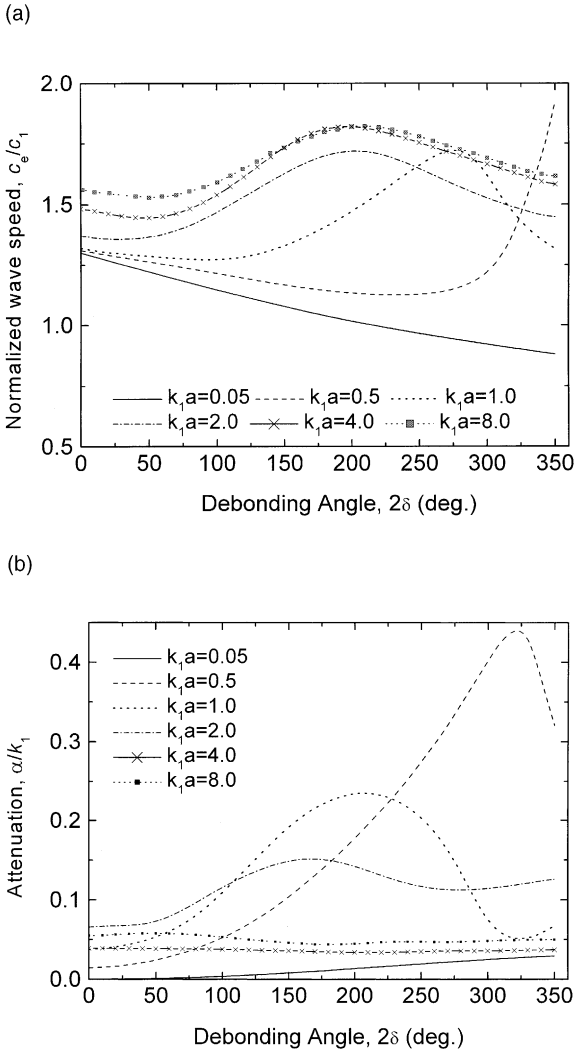

Fig. 6. Variations of wave speed and attenuation versus debonding angle at different frequencies: (a) normalized wave speed, (b) normalized attenuation.

$$u_1^{(0)} = \sum_{n=0}^{\infty} A_n H_n^{(1)}(k_1 r)\cos n(\theta + \theta_o), \tag{A.1}$$

$$u_2^{(0)} = \sum_{n=0}^{\infty} B_n J_n(k_2 r)\cos n(\theta + \theta_o), \tag{A.2}$$

where $J_n(x)$ is the first kind Bessel functions of order n. The scattering coefficients for each partial wave can be obtained by imposing the continuity conditions at the interface (Morse and Feshbach, 1953)

$$A_n = A\frac{\varepsilon_n \mathrm{i}^n}{D_n}\left[ZJ_n(k_1 a)J_n'(k_2 a) - J_n'(k_1 a)J_n(k_2 a)\right], \tag{A.3}$$

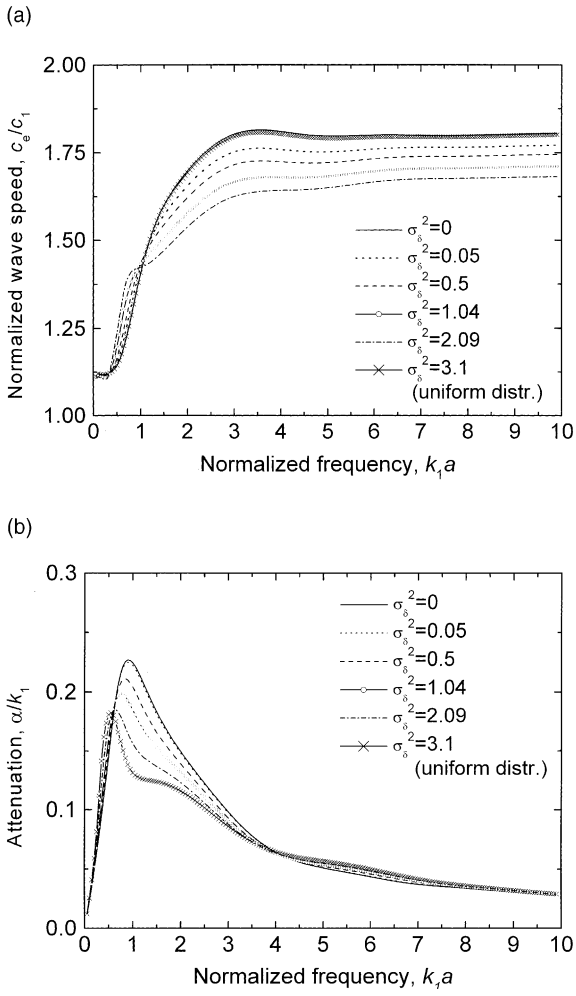

Fig. 7. Variations of wave speed and attenuation for mean debonding angle $2\bar{\delta} = 180°$ with $\sigma_\delta^2 = 0$, 0.05, 0.5, 1.04, 2.09 and 3.1 (uniform distribution): (a) normalized wave speed, (b) normalized attenuation.

$$B_n = A\frac{2\varepsilon_n \mathrm{i}^{n+1}}{\pi k_1 a D_n}, \tag{A.4}$$

where

$$D_n = H_n'^{(1)}(k_1a)J_n(k_2a) - ZH_n^{(1)}(k_1a)J_n'(k_2a), \tag{A.5}$$

$$Z = \frac{\mu_2 k_2}{\mu_1 k_1}. \tag{A.6}$$

The symmetric and antisymmetric parts of the additional interior fields can also be written similarly to the scattered ones (Eqs. (6) and (7))

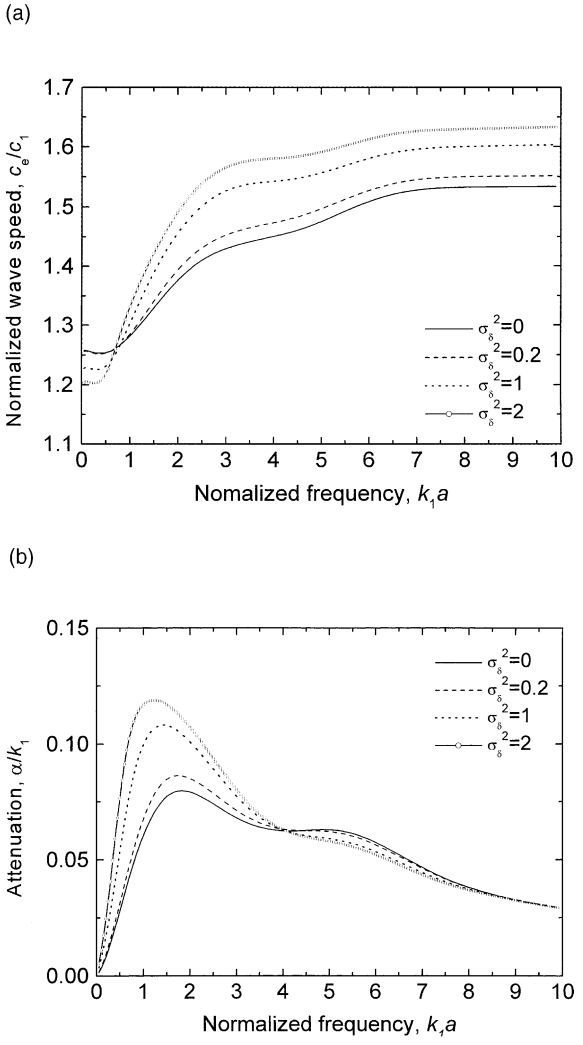

Fig. 8. Variations of wave speed and attenuation for mean debonding angle $2\bar{\delta} = 60°$ with $\sigma_\delta^2 = 0$, 0.2, 1 and 2: (a) normalized wave speed, (b) normalized attenuation.

$$u_{2S}^{(1)} = \sum_{n=0}^{\infty} F_n^{(S)} J_n(k_1 r)\cos n\theta, \tag{A.7}$$

$$u_{2A}^{(1)} = \sum_{n=1}^{\infty} F_n^{(A)} J_n(k_2 r)\sin n\theta. \tag{A.8}$$

The boundary conditions at the interface, $r = a$ are

$$u_1^{(1)} - u_1^{(2)} = \begin{cases} 0, & \delta \leqslant \theta \leqslant \pi \\ \Delta U(\theta), & 0 \leqslant \theta \leqslant \delta, \end{cases} \tag{A.9}$$

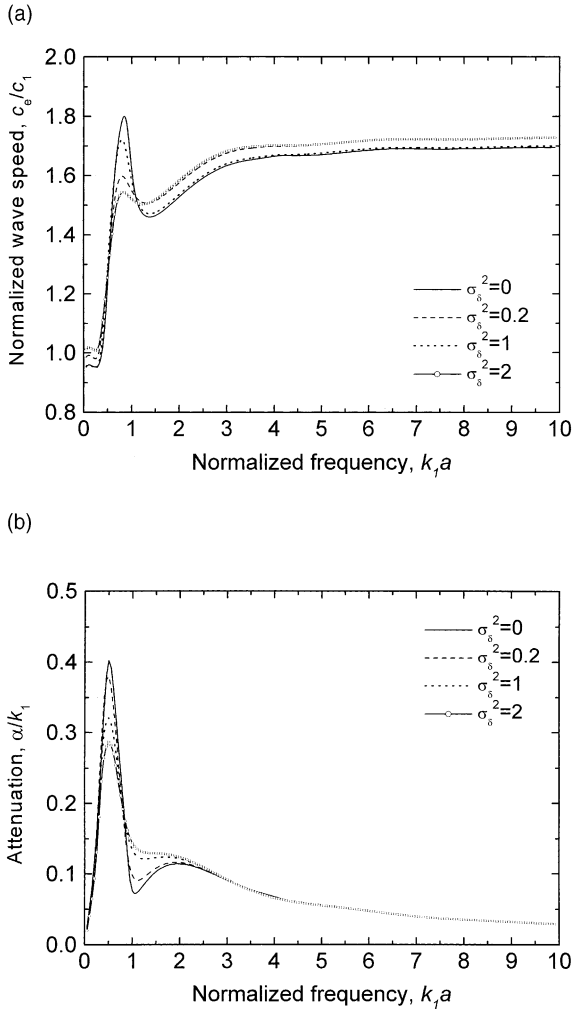

Fig. 9. Variations of wave speed and attenuation for mean debonding angle $2\bar{\delta} = 300°$ with $\sigma_\delta^2 = 0$, 0.2, 1 and 2: (a) normalized wave speed, (b) normalized attenuation.

$$\mu_1 \frac{\partial u_1}{\partial r} = \mu_2 \frac{\partial u_2}{\partial r}, \quad 0 \leqslant \theta \leqslant \pi, \tag{A.10}$$

$$\mu_1 \frac{\partial u_1}{\partial r} = \mu_2 \frac{\partial u_2}{\partial r} = 0, \quad 0 \leqslant \theta \leqslant \delta. \tag{A.11}$$

Here, $\Delta U(\theta)$ is the dynamic COD that is analogous to that in the static problem.

For symmetric problem, the COD is expanded using the symmetric Chevyshev orthogonal polynomials (Abramowitz and Stegun, 1965)

$$\Delta U_S(\theta) = \sum_{n=1}^{\infty} \beta_n^{(S)} \phi_n^{(S)}(\theta), \tag{A.12}$$

where

$$\phi_n^{(S)}(\theta) = \frac{1}{2n-1}\cos\left[(2n-1)\sin^{-1}\left(\frac{\theta}{\delta}\right)\right]. \tag{A.13}$$

From Eqs. (6) and (7), (A.1) and (A.2), and (A.7)–(A.12), the following system of linear equations for the coefficients of the symmetric COD is obtained,

$$\sum_{n=1}^{\infty} Q_{mn}^{(S)}\beta_n^{(S)} = N_m^{(S)}, \quad m = 1, 2, 3, \ldots \tag{A.14}$$

where

$$Q_{nm}^{(S)} = \frac{\delta^2}{8}\delta_{m1}\delta_{n1}\frac{H_0'^{(1)}(k_1a)J_0'(k_2a)}{D_0} + \sum_{p=1}^{\infty}\frac{H_p'^{(1)}(k_1a)J_p'(k_2a)}{p^2 D_p}J_{2n-1}(p\delta)J_{2m-1}(p\delta), \tag{A.15}$$

and

$$N_m^{(S)} = \frac{\delta}{2}\delta_{n1}J_0'(k_2a)B_0 + \sum_{p=1}^{\infty}\frac{B_p}{p}J_{2n-1}(p\delta)J_p'(k_2a)\cos p\theta_o. \tag{A.16}$$

Similarly, the antisymmetric COD coefficients can be expanded using the antisymmetric Chebyshev polynomials,

$$\Delta U_A(\theta) = \sum_{n=1}^{\infty}\beta_n^{(A)}\phi_n^{(A)}(\theta), \tag{A.17}$$

where

$$\phi_n^{(A)}(\theta) = \frac{1}{2n}\sin\left[2n\sin^{-1}\left(\frac{\theta}{\delta}\right)\right]. \tag{A.18}$$

The system of linear equations for the coefficients of antisymmetric COD is obtained,

$$\sum_{n=1}^{\infty} Q_{mn}^{(A)}\beta_n^{(A)} = N_m^{(A)}, \quad m = 1, 2, 3, \ldots \tag{A.19}$$

where

$$Q_{nm}^{(A)} = \sum_{p=1}^{\infty}\frac{H_p'^{(1)}(k_1a)J_p'(k_2a)}{p^2 D_p}J_{2n}(p\delta)J_{2m}(p\delta), \tag{A.20}$$

and

$$N_m^{(A)} = -\sum_{p=1}^{\infty}\frac{B_p}{p}J_{2n}(p\delta)J_p'(k_2a)\sin p\theta_o. \tag{A.21}$$

As can be expected naturally, it is noted that the system matrices $Q_{mn}^{(S)}$ and $Q_{mn}^{(A)}$ are independent of the incident angle θ_o while the excitation vectors $N_m^{(S)}$ and $N_m^{(A)}$ are dependent on the incident angle. From the COD expansion coefficients $\beta^{(S),(A)}$, the scattering coefficients can be obtained as follows:

$$E_0^S = -\frac{Z}{4}\frac{J_0'(k_2a)}{D_0}\delta\beta_1^{(S)}, \tag{A.22}$$

$$E_n^S = -\frac{Z}{n}\frac{J_n'(k_2a)}{D_n}\sum_{m=1}^{\infty}J_{2m-1}(m\delta)\beta_m^{(S)}, \tag{A.23}$$

$$E_n^{\mathrm{A}} = -\frac{Z}{n}\frac{J_n'(k_2 a)}{D_n}\sum_{m=1}^{\infty} J_{2m}(m\delta)\beta_m^{(\mathrm{A})} \tag{A.24}$$

Appendix B. Truncated Gaussian distribution

The truncated Gaussian distribution (Bendat and Piersol, 1986) can be used for the case that the domain of the random variables is finite but still the distribution characteristic is quite similar to the ordinary Gaussian distribution. To define the truncated Gaussian probability density function (PDF) one can start with the ordinary Gaussian PDF defined over $\{-\infty,\infty\}$,

$$p_1(x) = \frac{\exp[-(x-\mu_x)^2/2\sigma_x^2]}{\sigma_x\sqrt{2\pi}}, \tag{B.1}$$

where μ_x is the mean and σ_x is the standard deviation of the random variable x.

The truncated Gaussian PDF for a random variable x in a finite range $\{x_1,x_2\}$ can be defined

$$p(x) = \begin{cases} = Cp_1(x), & x_1 < x < x_2 \\ = 0, & \text{otherwise}, \end{cases} \tag{B.2}$$

where

$$C = \frac{1}{\int_{x_1}^{x_2} p_1(x)\,\mathrm{d}x}. \tag{B.3}$$

Therefore,

$$p(x) = \frac{2\exp[-(x-\mu_x)^2/2\sigma_x^2]}{\sigma_x\sqrt{2\pi}\left[\mathrm{erf}\left(\frac{x_2-\mu_x}{\sigma_x\sqrt{2}}\right) - \mathrm{erf}\left(\frac{x_1-\mu_x}{\sigma_x\sqrt{2}}\right)\right]}. \tag{B.4}$$

where $\mathrm{erf}(z)$ is the error function defined as (Abramowitz and Stegun, 1965)

$$\mathrm{erf}(z) = \frac{2}{\sqrt{\pi}}\int_0^z \mathrm{e}^{-t^2}\,\mathrm{d}t. \tag{B.5}$$

References

Abramowitz, M., Stegun, I.A., 1965. Handbook of Mathematical Functions. Dover, New York.

Angel, Y.C., Achenbach, J.D., 1991. Attenuation and speed of antiplane waves in a cracked solid using the Kramers–Kronig relations. J. Acoust. Soc. Am. 90, 2757–2762.

Beltzer, A.I., Brauner, N., 1985. SH-waves of an arbitrary frequency in random fibrous composites via the K–K relations. J. Mech. Phys. Solids 33, 471–475.

Beltzer, A.I., Brauner, N., 1986. The causal effective field approach – application to elastic waves in random composites. Mech. Matr. 5, 161–169.

Beltzer, A.I., Brauner, N., 1987. The dynamic response of random composites by a causal differential method. Mech. Matr. 6, 337–345.

Bendat, J.S., Piersol, A.G., 1986. Random Data. Wiley, New York.

Bohren, C.F., Gilra, D.P., 1979. Extinction by a spherical particle in an absorbing medium. J. Coll. Interf. Sci. 72, 215–221.

Benveniste, Y., Aboudi, J., 1984. A continuum model for fiber reinforced materials with debonding. Int. J. Solids Struct. 20, 935–951.

Bose, S.K., Mal, A.K., 1973. Longitudinal shear waves in fiber-reinforced composite. Int. J. Solids Struct. 9, 1075–1085.

Johnson, W.S., 1989. Fatigue testing and damage development in continuous fiber reinforced metal matrix composites. In: Johnson, W.S. (Ed.), Metal Matrix Composites: Testing, Analysis, and Failure Modes, ASTM STP 1032, ASTM, Philadelphia, pp. 194–221.

Kim, J.-Y., 1999. Multiple scattering and propagation of elastic waves in discrete random composites. Mech. Mater., in press.
Kim, S.Y., Moon, H.J., Earmme, Y.Y., 1995. Effective elastic moduli in fiber reinforced composite with circular are shaped interfacial cracks. Int. J. Fract. 71, 85–93.
Liu, W., Kriz, R., 1997. Shear waves in fiber-reinforced composites with interfacial cracks. Int. J. Solids Struct. 35, 1425–1449.
Morse, P.M., Feshbach, H., 1953. Methods of Theoretical Physics. McGraw Hill, New York.
Norris, A.N., 1985. A differential scheme for the effective moduli of composites. Mech. Mat. 4, 1–16.
Teng, H., 1992. Effective longitudinal shear modulus of a unidirectional fiber composite containing interfacial cracks. Int. J. Solids Struct. 29, 1581–1595.
Waterman, P.C., Truell, R., 1961. Multiple scattering of elastic waves. J. Math. Phys. 2, 512–537.
Weaver, R.L., Pao, Y.-H., 1981. Dispersion relations for linear wave propagation in homogeneous and inhomogeneous media. J. Math. Phys. 22, 1909–1918.
Yang, Y., Norris, A.N., 1991. Shear wave scattering from a debonded fibre. J. Mech. Phys. Solids 39, 273–294.
Yuan, F.G., Pagano, N.J., Cai, X., 1997. Elastic moduli of brittle matrix composites with interfacial debonding. Int. J. Solids Struct. 34, 177–201.
Zhang, C.H., Gross, D., 1993. Wave attenuation and dispersion in randomly cracked solids – I. Slit cracks. Int J. Engng Sci. 31, 841–858.